Pathological Alterations in the Gastrointestinal Tract of a Porcine Model of DMD

Xiaodong Zhou
Jilin University

Hongsheng Ouyang
Jilin University

Daxin Pang
Jilin University

Renzhi Han (renzhi.han@osumc.edu)
Ohio State University Wexner Medical Center Department of Surgery https://orcid.org/0000-0002-8202-9186

Xiaochun Tang
Jilin University

Research

Keywords: CRISPR, Duchenne muscular dystrophy, genome editing, gastrointestinal tract, pig, porcine, swine

Posted Date: March 8th, 2021

DOI: https://doi.org/10.21203/rs.3.rs-267849/v1

Version of Record: A version of this preprint was published at Cell & Bioscience on July 15th, 2021. See the published version at https://doi.org/10.1186/s13578-021-00647-9.

Pathological alterations in the gastrointestinal tract of a porcine model of DMD

Xiaodong Zou[1], Hongsheng Ouyang[1], Daxin Pang[1], Renzhi Han[2,*], Xiaochun Tang[1,*]

[1]Jilin Provincial Key Laboratory of Animal Embryo Engineering, College of Animal Sciences, Jilin University, Changchun, Jilin Province, People's Republic of China

[2]Department of Surgery, Davis Heart and Lung Research Institute, Biomedical Sciences Graduate Program, Biophysics Graduate Program, The Ohio State University Wexner Medical Center, Columbus, OH 43210

*Address correspondence to:
Renzhi Han, Ph.D.
Department of Surgery
Davis Heart and Lung Research Institute
The Ohio State University Wexner Medical Center
Columbus, OH 43210
Phone: (614) 685-9214
E-mail: renzhi.han@osumc.edu

Or

Xiaochun Tang, Ph.D.
Jilin Provincial Key Laboratory of Animal Embryo Engineering
College of Animal Sciences
Jilin University
Changchun, Jilin Province
People's Republic of China
E-mail: xiaochuntang@jlu.edu.cn

Abstracts

Patients with Duchenne muscular dystrophy (DMD) develop severe skeletal and cardiac muscle pathologies, which result in premature death. Therefore, the current therapeutic efforts are mainly targeted to correct dystrophin expression in skeletal muscle and heart. However, it was reported that DMD patients may also exhibit gastrointestinal and nutritional problems. How the pathological alterations in gastrointestinal tissues may contribute to the disease are not fully explored. Here we employed the CRISPR/Cas9 system combined with somatic nuclear transfer technology (SCNT) to establish a porcine model of DMD and explored their pathological alterations. We found that genetic disruption of dystrophin expression led to morphological gastrointestinal tract alterations, weakened the gastrointestinal tract digestion and absorption capacity, and eventually led to malnutrition and gastric dysfunction in the DMD pigs. This work provides important insights into the pathogenesis of DMD and highlights the need to consider the gastrointestinal dysfunction as an additional therapeutic target for DMD patients.

Keywords: CRISPR; Duchenne muscular dystrophy; genome editing; gastrointestinal tract; pig; porcine; swine

Declarations

Funding

This work was supported by grants from the National Key Research and Development Program of China Stem Cell and Translational Research (2019YFA0110702), National Natural Science Foundation of China (No. 31572345), the Program for JLU Science and Technology Innovative Research Team (2017TD-28). R.H. is supported by the National Heart, Lung and Blood Institute grant [HL116546]; and the Parent Project Muscular Dystrophy award.

Conflicts of interest

The authors declare that they have no conflict of interests.

Ethics approval

All animal studies were approved by the Animal Welfare and Research Ethics Committee at Jilin University, and all procedures were conducted strictly in accordance with the Guide for the Care and Use of Laboratory Animals. All surgeries were performed under anesthesia, and every effort was made to minimize pain and stress (**SY201901013**).

Consent to participate

Not applicable.

Consent for publication

All co-authors have reviewed and approved of the manuscript prior to submission. The manuscript has been submitted solely to this journal and is not published, in press, or submitted elsewhere.

Availability of data and material

All relevant data supporting the key findings of this study are available within the article and its Supplementary Information files or from the corresponding author upon reasonable request.

Code availability

Not applicable.

Authors' contributions

R.H., X.Z., H.O. and X.T. conceived the study and wrote the manuscript. X.Z. and X.T. performed the experiments, analyzed the data and drafted the manuscript.

Introduction

Duchenne muscular dystrophy (DMD), inherited in an X-linked recessive manner, is a severe and progressive neuromuscular disorder[1], and its prevalence in the general population is approximately 1/5000[2, 3]. Progressive muscle injury and degeneration in DMD patients leads to muscular weakness, loss of ambulation, respiratory impairment, and cardiomyopathy[4]. Most patients become wheelchair-bound in childhood and heavily depend on their caregivers for their daily life[5]. Although the clinical and pathological progression of skeletal muscle and myocardium involvement can be variable, death usually occurs around the age of 30 years due to cardiac and/or respiratory failure[6].

DMD is caused by mutations in the *DMD* gene located at Xp21, which codes for the dystrophin protein[7], a cytoskeletal protein that functions in the muscle force transmission and sarcolemmal stability of muscle fibers[8]. The *DMD* gene is one of the largest genes in the human genome, containing 79 exons spanning 2.5 Mb of the genomic DNA[9, 10]. Most of the mutations are due to deletions or duplications with point mutations accounting for less than 10% of the cases[11, 12]. “Hot spots” for these mutations are located in the regions of exons 3-7 and exons 45-55[11]. *DMD* exon 51 has been the most studied target in both preclinical and clinical settings, and the availability of standardized procedures to quantify exon skipping would be beneficial for the evaluation of preclinical and clinical data[13].

With the advancing pathological progress of DMD, patients often suffer from gastrointestinal or nutritional complications, evidenced by mandibular contracture, swallowing impairment, dietary or nutrient imbalance, fluid imbalance, low bone density and weight gain or loss[14]. In the *mdx* mouse, the most commonly used animal model of DMD, the expression of neuronal nitric oxide synthase (nNOS) in colonic smooth muscle cells is decreased, the contractile ability of the colon is weakened, the transport speed of the small intestine is delayed, and fecal excretion is reduced[15]. In addition, *mdx* mice have a higher concentration of collagen fibers in the submucosal region of the gastrointestinal tract than wild-type (WT) mice. These alterations are presumably consequences of the loss of dystrophin protein[15-17]. Therefore, understanding the functional and morphological alterations of the gastrointestinal tract in DMD could have important implications for therapeutic interventions. However, the overall disease alterations in *mdx* mice are much less intense than those observed in DMD patients. For example, *mdx* mice exhibit only a slightly shortened life span and no apparent clinical signs of muscular dystrophy[18, 19].

Like humans, pigs are true omnivores, and their balanced nutritional requirements are particularly similar to the dietary requirements of humans[20]. Of the available animal models, pigs exhibit the closest time required for intestinal transformation and digestive efficiency to those in humans[21]. Pigs are, in many ways, attractive models that closely mimic human physiology and pathology[22]. Therefore, in this study, we used the CRISPR/Cas9 technology to create a porcine model of DMD by targeting

DMD exon 51 and reported the pathological alterations in the gastrointestinal tract of these animals.

Results

Design of the *DMD* gene targeting strategy

The dystrophin protein shares a high homology among species. Amino acid sequence alignment results revealed that the porcine dystrophin protein is highly homologous to the human dystrophin protein with 94.16% homology (**Suppl. Fig. 1A**). We designed a sgRNA targeting pig *DMD* exon 51 (**Suppl. Fig. 1B**). The on-target editing efficiency of this sgRNA was assessed by Sanger sequencing of the target site PCR amplicon following electroporation into porcine fetal fibroblasts (PFFs). Multipeaks around the Cas9 cleavage site were observed, indicating that this sgRNA is effective in targeting *DMD* exon 51 (**Suppl. Fig. 1C**). To assess the off-target activity, we selected the top eight potential off-target sites for this sgRNA identified by in silico analysis, and sequenced the PCR amplicons for all these 8 sites. No overlapping peaks were found in the sequencing traces, suggesting that the editing activities at these potential off-target sites remain undetectable for the sensitivity of this assay (**Suppl. Fig. 1D, Table 1 and 2**).

PFFs with engineered mutations in *DMD* exon 51 showed impaired cell membrane integrity and early apoptosis

PFFs with *DMD* exon 51 disruption following electroporation were chosen as the donor

158 cells for somatic nuclear transfer. A total of 400 individual PFF cell clones were
159 analyzed and 113 (27.5%) were found to carry seven different types of mutations (**Fig.**
160 **1A，Suppl. Table 3**). All mutation types of PFFs showed abnormalities in the mRNA
161 and protein levels of the *DMD* gene (**Suppl. Fig. 2A, B**).
162
163 Previous research showed that dystrophin protein functions to stabilize the integrity of
164 the muscle fiber membrane. To examine whether the mutations in PFFs induced by
165 the CRISPR/Cas9 system disrupt cell membrane integrity, we performed neutral red
166 dye (NRD) uptake and lactate dehydrogenase (LDH) release assays. As shown in **Fig.**
167 **1B** and **Suppl. 2C,** the NRD uptake of PFFs with mutations in *DMD* exon 51 was
168 significantly lower than that of PFFs from the control group, suggesting that the *DMD*
169 mutant PFFs have lower viability. Consistent with the results of the NRD uptake assay,
170 the LDH activity was remarkably elevated in the culture medium of PFFs with *DMD*
171 exon 51 mutations compared to that in the culture medium of control PFFs (**Fig. 1C,**
172 **Suppl. 2D**). Increasing evidence has shown that apoptosis and autophagy may play
173 important roles in DMD. Therefore, we compared apoptosis and autophagy between
174 gene-edited and WT PFFs. As shown in **Fig. 1D, Suppl. Fig. 2E and 2F,** increased
175 early apoptosis in PFFs carrying mutations in *DMD* exon 51 was observed as
176 compared to control PFFs. By assaying the conversion of LC3B-I to LC3B-II, we found
177 no evidence of increased autophagy in gene-edited PFFs **(Fig. 1E)**. Finally, we found
178 no significant differences in blastocyst development rate between the control and
179 gene-edited PFFs (**Suppl. Fig. 2G, H; Suppl. Table 4**). These results demonstrated

that *DMD* exon 51 disruption led to a compromised cell membrane integrity and caused early apoptosis but did not affect the developmental potential of PFFs.

Generation of Bama miniature pigs with *DMD* exon 51 mutations

Fig. 2A shows the flowchart of the construction process of Bama miniature pigs with *DMD* exon 51 mutations (DMD-delE51 pigs). Large white pigs were selected as surrogate sows, and a total of 200 embryos were transferred to each surrogate. In total, three pregnant surrogates were carried to term, and 15 piglets were delivered (**Suppl. Table 5**). DNA gel electrophoresis and sequencing analysis of all piglets showed that 9 of the newborns carried mutations at the target locus (**Fig. 2B, C**). To examine whether the *DMD* mutations in pigs disrupt the expression of the *DMD* gene, we performed RT-PCR analysis of *DMD* gene expression. As shown in **Fig. 2D**, the expression of the *DMD* gene in the cardiac and skeletal muscle of DMD-delE51 pigs was significantly lower than that of WT pigs. To further examine the expression of dystrophin protein in the muscle of these pigs, we performed Western blotting and immunohistochemistry staining. Compared with WT controls, the expression of dystrophin protein in DMD-delE51 pigs was disrupted (**Fig. 2E, F**). These results demonstrated that the mutations in *DMD* exon 51 disrupted the expression of the *DMD* gene and dystrophin protein.

Muscular dystrophy and cardiomyopathy presentation in DMD-delE51 pigs

As shown in **Fig. 3A**, the DMD-delE51 pigs exhibited obvious hindlimb paralysis

compared with their WT littermates. The DMD-delE51 pigs began to die postnatally, with the mortality rate reaching 100% within 12 weeks, whereas WT piglets had a normal lifespan (**Fig. 3B**). To examine the histopathology of the DMD-delE51 pigs, we performed H&E staining of cardiac, diaphragm and gastrocnemius muscle sections from the pigs at 12 weeks of age. As shown in **Fig. 3C**, the cardiac muscle sections of DMD-delE51 pigs displayed irregularly arranged and cracked myocardial fibers, significantly widened fibrous gaps and hypertrophic myocardial fibers. Meanwhile, typical muscular dystrophy signs were observed in skeletal muscles, as evidenced by increased fiber size variation, centrally nucleated fibers and inflammatory cell infiltration (**Fig. 3D, E**). As shown in **Fig. 3G, I,** the average fiber area of the diaphragm and gastrocnemius muscles of DMD-delE51 pigs was significantly lower than that of WT pigs due to the cycles of degeneration and regeneration. In addition, a significantly increased percentage of muscle fibers with central nuclei was observed in DMD-delE51 pigs, as shown in **Fig. 3H** and **3J**, and fiber size distribution revealed a significant increase in smaller fibers (**Fig. 3K, L**). Moreover, muscular dystrophy and cardiomyopathy biomarkers were founded elevated in the serum samples of DMD-delE51 pigs. As shown in **Fig. 3F**, DMD-delE51 pigs exhibited significantly elevated levels of serum creatine kinase (CK), creatine kinase MB isoenzyme (CKMB), cardiac troponin T (cTn-T), myoglobin (Mb), α-hydroxybutyrate dehydrogenase (α- HBDH) LDH compared with WT pigs ($P<0.001$, ***; $0.001<P<0.01$, **). Taken together, these results demonstrated that the DMD-delE51 pigs developed DMD and cardiomyopathy.

Pathological alterations in the small intestine linked to malnutrition in DMD-delE51 pigs

The growth and development of DMD-delE51 pigs and WT pigs were monitored. Compared with their WT littermates, DMD-delE51 pigs exhibited smaller body size (**Fig. 4A**) and lighter body weight (**Fig. 4B**). Subsequent serological tests showed that the levels of serum albumin (ALB) and prealbumin (PA) were significantly reduced in DMD-delE51 pigs, indicating malnutrition (**Fig. 4C, D**). To further examine the histopathology of the DMD-delE51 pigs, we performed H&E staining of small intestinal tissue sections from the pigs at 12 weeks of age. As shown in **Fig. 4E, 4G and Suppl. Fig. 3A,** compared with that of the controls, the intestinal villus height of DMD-delE51 pigs was significantly decreased, and the ratio of villus height to crypt depth was approximately 60% reduced. Meanwhile, the thickness of the intestinal wall was reduced by approximately 40% (**Fig. 4F**). In addition, we also examined the expression of the *DMD* gene and dystrophin protein in the small intestine. The expression of the *DMD* gene and dystrophin protein were significantly disrupted in the stomach and small intestine (**Suppl. Fig. 3B-E**).

DMD-delE51 pigs suffered from gastric dysfunction

H&E staining of the stomach revealed that the gastric gland of DMD-delE51 pigs was significantly thinner than that of WT pigs (**Fig. 5A, B**). Importantly, compared with WT pigs, serum gastrin 17 (G-17) levels in DMD-delE51 pigs were significantly downregulated at week 7 (**Fig. 5C**), serum pepsinogen I (PGI) levels were upregulated

at week 6 and reached the peak at week 8, but then sharply declined to a minimum by week 12 (**Fig. 5D**). Serum pepsinogen II levels began to be significantly upregulated at week 7 and remained higher than those in WT pigs (**Fig. 5E**). The ratio of PGI/PGII (PGR) at week 7 was significantly lower in DMD-delE51 pigs than in WT pigs (**Fig. 5F**). Collectively, DMD-delE51 pigs with disrupted dystrophin expression exhibited morphological abnormality and functional impairment in the stomach.

Discussion

DMD is a fatal disease with multisystem involvement. Existing mouse[23], rat[24, 25], rabbit[26], dog[27], pig[28-31] models have been instrumental to understand the pathogenesis of DMD and to develop therapeutic strategies. In this study, we established a new pig model of DMD using CRISPR-genome editing and SCNT, and studied the pathology in skeletal muscle, heart, stomach and small intestine. We demonstrated that the DMD-delE51 pigs were born with abnormal posture, developed muscular dystrophy, cardiomyopathy and gastrointestinal defects, and died within 12 weeks. In DMD patients, weakness and difficulty in ambulation are first noted between 3 and 7 years old[8]. A waddling gait is common, and patients become wheelchair-bound by the age of 12[32]. Death usually occurs in the third decade of life due to heart or respiratory failure. Our suggest that DMD-delE51 pigs have a markedly accelerated disease progression as compared with that of DMD patients, similar to the other pig model of DMD reported earlier[28-31].

Individuals with DMD often have gastrointestinal or nutritional impairments[33]. Previous research has demonstrated that the fundic gland and intestinal wall are the most important parts of the digestive system[34]. The thickness of the fundic gland and intestinal wall is closely related to the rhythmic contraction of the gastrointestinal tract and mechanical digestion and reflects the rates of digestion and absorption of nutrients. Moreover, the ratio of villus height to crypt depth comprehensively reflects the digestive and absorption function of the small intestine[35]. When the ratio decreases, the mucous membrane is likely to be damaged, and the digestive and absorptive capacity is reduced, often accompanied by diarrhea and growth inhibition[36]. In this study, DMD-delE51 pigs showed decreased gastric fundic gland and intestinal wall thickness and shortened intestinal villus height. Our findings indicate that DMD-delE51 pigs have abnormal digestion and absorption in the gastrointestinal tract, leading to malnutrition. Previous studies demonstrated abnormal levels of G-17, PGI, PGII and PGR in serum of patients with gastritis[37]. Notably, the changes of G-17, PGI and PGII in DMD-delE51 pigs were highly consistent with those in human patients with atrophic gastritis (AG)[38]. In AG dominated by antral atrophy, antral mucosal atrophy can lead to a decrease in the number of G cells and a decrease in the secretion of G-17, resulting in a decrease in the content of G-17 in blood circulation[39]. Studies have shown that low levels of serum PGI and PGR are biological markers of gastric body atrophy, and the level of serum PGI decreases gradually with increasing severity of mucosal atrophy[40]. Therefore, our findings suggest that DMD-delE51 pigs developed gastric dysfunction, which likely contributes to the accelerated disease progression.

Previous studies have reported that the clinical manifestations of gastric dilatation and intestinal pseudo-obstruction in patients with DMD are potentially related to the lack of dystrophin in muscle[41]. We found that dystrophin was expressed in the gastrointestinal tissues of WT pigs but disrupted in DMD-delE51 pigs, suggesting that the loss of dystrophin protein is likely involved in the pathological alterations of the gastrointestinal tract, weakening the digestion and absorption capacity of the gastrointestinal tract and eventually inducing malnutrition and gastric dysfunction in DMD-delE51 pigs.

The gastrointestinal dysfunction is of clinical importance and likely contributes to the overall disease progression. As the life expectancy of DMD patients increases due to better management of the life-threatening complications, the gastrointestinal dysfunction could become more significant. It is thus necessary to consider the gastrointestinal track as a therapeutic target organ for DMD patients.

Materials and Methods

Ethics statement

All animal studies were approved by the Animal Welfare and Research Ethics Committee at Jilin University, and all procedures were conducted strictly in accordance with the Guide for the Care and Use of Laboratory Animals. All surgeries were performed under anesthesia, and every effort was made to minimize animal suffering

(**SY201901013**).

Construction of Cas9/sgRNA targeting vector

The CRISPR/Cas9 system was constructed as previously described[42]. Briefly, the plasmid containing the U6-sgRNA and Cas9 expression elements was obtained from Addgene (#42230). The targeting sgRNA is CTTGGACAGAACTTACCGAC. A pair of complementary sgRNA oligo DNAs were synthesized, annealed into double-strand DNAs, and ligated to the *BbsI* sites of the vector to form the intact plasmid, which was confirmed by sequence analysis.

Isolation and culture of PFFs

The isolation and culture of PFFs were performed as previously described[43]. Thirty-three-day-old fetuses were chosen and separated from Bama miniature sows. First, fetuses, without the head, tail, limb bones, and viscera, were cut into small pieces. Then, these small pieces were digested and cultured in DMEM (GIBCO) supplemented with 15% fetal bovine serum (FBS) at 39 °C and 5% CO_2 in a humidified incubator. PFFs at passage 1 were frozen in FBS containing 10% dimethyl sulfoxide (DMSO).

Electrotransfection and single-cell colony selection

First, PFFs were thawed and cultured in 10-cm culture dishes. Then, $3x10^6$ PFFs were electrotransfected with 200 μL of Opti-MEM (GIBCO) using 2-mm gap cuvettes and a

BTX ECM 2001 electroporator. The parameters for electrotransfection were as follows: 340 V, 1 ms, 3 pulses for 1 repeat. During these experiments, a total of 30 μg plasmids were added to the reaction media. At 36 h after electrotransfection, the cells were plated into ten 10-cm dishes at a density of $4x10^3$ cells per dish. Single-cell colonies were picked and cultured in 24-well plates. When the plates reached 90% confluence, 10% of cells from each plate was lysed using 10 μL of lysis buffer (0.45% NP-40 plus 0.6% Proteinase K) for 60 min at 56 °C and then 10 min at 95 °C. The lysate was used as a template for PCR. The forward and reverse primers were 5'-CAGCTAAACAGAGTAAAGAG-3' and 5'-GATTTCCCTAGAGTCCACTT-3', respectively. The PCR conditions were 94 °C for 5 min; 94 °C for 30 s, 55 °C for 30 s, and 72 °C for 1 min for 35 cycles; 72 °C for 5 min; and hold at 16 °C. The PCR products were sequenced, and some PCR products were ligated into the PLB vector (Tiangen, Beijing, China) and sequenced to identify the mutations. The positive cell colonies were expanded and cryopreserved.

Off-target assay

Potential off-target sites (OTSs) were predicted by scanning the porcine genome using BLAST based on the homology to the sgRNA plus protospacer adjacent motif (PAM). The genomic DNA of the mutant cell clones was analyzed via PCR and DNA sequencing to determine the target effects. The primer sequences used for analyzed the off-target activities are listed in **Suppl. Table 2**.

Somatic nuclear transfer technology (SCNT) and genotyping of mutant piglets

Somatic cell nuclear transfer and embryo transfer were performed as previously reported[44]. Positive colonies were screened and selected as donor cells for SCNT. First, a single donor cell was microinjected into the enucleated pig oocyte. Second, reconstructed embryos were electroactivated. Finally, embryos were transferred into synchronized recipient pigs. After piglets were delivered, genomic DNA samples were extracted from the tail tissue for genotyping.

Survival curve and bodyweight

The bodyweights of age- and sex-matched WT and *DMD*-modified pigs were measured biweekly. A minimum of three individual animals of *DMD*-modified pigs was used in all experiments.

Serum biochemical analysis

After piglets were born, serum samples were collected and measured by enzyme-linked immunosorbent assay (ELISA) following the manufacturer's instructions, in an infinite 200 PRO Microplate Reader (Tecan, Switzerland). Samples were measured in triplicate, and the absorbance was monitored at 37 °C.

Neutral red dye (NRD) uptake assay

The cell viability was analyzed by the Neutral Red Cell Proliferation and Cytotoxicology Assay Kit (Beyotime, China). The absorbance (OD) was measured at 540 nm, and the

value at the reference wavelength of 630 nm was subtracted. The assay was performed on each cell clone in triplicate, and values were averaged from 4–6 wells per plate.

Lactate dehydrogenase (LDH) assay

LDH activity in the medium was measured using the LDH assay kit (Beyotime, China) according to the manufacturer's instruction. The OD was measured by an infinite 200 PRO Microplate Reader (Tecan, Switzerland) at a wavelength of 490 nm. LDH activity was calculated according to the formula provided by the instruction.

Analysis of apoptotic cells by flow cytometry

Annexin V-FITC antibody immunofluorescence combined with propidium iodide (PI) was used to perform a fluorescent analysis of apoptosis, according to the instructions of the Annexin V-FITC apoptosis detection kit (Beyotime, China). A total of 1×10^5 cells were collected and incubated with Annexin V-FITC and PI in the provided binding buffer for 25 min in the dark at 4 ˚C, and analyzed by flow cytometry.

Western blotting

Equal amounts of proteins were separated through SDS-PAGE on a 5% separating gel, and the protein bands were electrophoretically transferred to polyvinylidene fluoride (PVDF) membranes. Then, the membranes were blocked for 2 h in TBST buffer with 5% milk at room temperature. The membranes were subsequently

incubated with the primary antibodies (rabbit anti-light chain-3B (LC3B) antibody, BM4827, Boster, 1:400; anti-dystrophin antibody, ab15277, Abcam, 1:400) overnight at 4°C. After wash 3 times for 10 min with TBST buffer, the membranes were incubated for 1 h with the secondary antibody. Finally, the protein bands were detected with the ECL-Plus Western blotting reagent.

Quantitative reverse transcription PCR (RT-PCR)

For detection of relative mRNA expression of the *DMD* gene, total RNA was isolated from muscle samples using TRNzol-A$^+$ Reagent (TIANGEN, DP421) following the manufacturer's recommendations. The RNA (1 μg) was reverse-transcribed (RT) to generate cDNA using a FastKing RT Kit (with gDNase) (TIANGEN, KR116) according to the manufacturer's manual. The reaction conditions were 95 °C for 5 min and 10 s; 60 °C for 20 s and 72 °C for 30 s for 40 cycles; and 95-55 °C for 30 s (melting curve). The fluorescence intensity and amplification plots were analyzed by a BIO-RAD iCycler Thermal Cycler with iQ5 Optical Module for RT-PCR (Bio-Rad, ABI 7500, iQ5). The results were expressed via the comparative cycle threshold (CT) method as described before, and expression levels were represented by fold changes over values derived from healthy pigs. *GAPDH* was utilized as a reference gene. The primers used in RT-PCR are listed in **Suppl. Table 6.**

Immunohistochemistry (IHC)

Dystrophin expression and location were examined in fixed sections. Muscle samples

were fixed in 4% paraformaldehyde (PFA), embedded in paraffin, and sectioned at 5 μm after harvest. IHC was performed according to standard techniques. Briefly, muscle sections were deparaffinized, and antigen retrieval was performed. After slices were cooled to 25 °C and washed twice with PBS, the slides were blocked with 5% BSA for 15 min at 25 °C. Then, the slides were incubated with the primary anti-dystrophin antibody (MANDYS8, GeneTex, 1:400) overnight at 4 °C. Following incubation and 3 washes with 0.05% Tween-20 in PBS, sections were incubated with Alexa Fluor 488-conjugated Affinipure goat anti-mouse IgG (H+L) (SA0006-1, ProteinTech, 1:100) for 1 h at 25 °C and washed again. Slides were mounted with SlowFade Gold Antifade Reagent with DAPI (Invitrogen). For analysis of protein abundance following IHC, 5 nonoverlapping pictures were randomly taken from each section.

Hematoxylin and eosin (H&E) staining

Fresh tissues including heart, gastrocnemius, diaphragm, stomach and intestine, were fixed in 4% PFA, embedded in paraffin, and sectioned at 5 μm. H&E staining was performed with standard techniques. Briefly, sections were incubated in Mayer's hematoxylin. Then, sections were rinsed with tap water and counterstained with 1% eosin. Finally, the sections were dehydrated, and coverslips were applied. Five nonoverlapping pictures were randomly taken from each muscle section.

Morphometric analysis of muscle

Morphometric analyses were performed on H&E-stained muscle sections of *DMD* exon 51-modified pigs and age-matched WT controls following the manufacturer's instructions, and five different regions were counted per section. The fiber size and percentage of central nucleated fibers were calculated by ImagePro Plus software (v6.0, Media Cybernetics, Silver Spring, MD, USA).

Statistical analysis

All data are expressed as the means ± standard error of the mean (SEM), and Student's *t*-test was used for statistical analysis. A single asterisk indicates statistical significance at $P<0.05$. Double asterisks indicate a strong statistical significance at $P<0.01$. Triple asterisks indicate even stronger statistical significance at $P<0.001$. All statistical analyses were completed using GraphPad Prism 7.0 software.

References

1. Moser, H. Duchenne Muscular-Dystrophy - Pathogenetic Aspects and Genetic Prevention. *Hum Genet* **66**, 17-40 (1984).
2. Mendell, J.R. & Lloyd-Puryear, M. Report of MDA muscle disease symposium on newborn screening for Duchenne muscular dystrophy. *Muscle Nerve* **48**, 21-26 (2013).
3. Moat, S.J., Bradley, D.M., Salmon, R., Clarke, A. & Hartley, L. Newborn bloodspot screening for Duchenne muscular dystrophy: 21 years experience in Wales (UK). *Eur J Hum Genet* **21**, 1049-1053 (2013).
4. Mercuri, E. & Muntoni, F. Muscular dystrophies. *Lancet* **381**, 845-860 (2013).
5. Birnkrant, D.J. et al. The respiratory management of patients with duchenne muscular dystrophy: a DMD care considerations working group specialty article. *Pediatr Pulmonol* **45**, 739-748 (2010).
6. Kohler, M. et al. Disability and survival in Duchenne muscular dystrophy. *J Neurol Neurosurg Psychiatry* **80**, 320-325 (2009).
7. Hoffman, E.P., Brown, R.H., Jr. & Kunkel, L.M. Dystrophin: the protein product of the Duchenne muscular dystrophy locus. *Cell* **51**, 919-928 (1987).
8. Blake, D.J., Weir, A., Newey, S.E. & Davies, K.E. Function and genetics of dystrophin and dystrophin-related proteins in muscle. *Physiol Rev* **82**, 291-329 (2002).
9. Coffey, A.J. et al. Construction of a 2.6-Mb Contig in Yeast Artificial Chromosomes Spanning the Human Dystrophin Gene Using an Sts-Based

Approach. *Genomics* **12**, 474-484 (1992).

10. Monaco, A.P., Walker, A.P., Millwood, I., Larin, Z. & Lehrach, H. A yeast artificial chromosome contig containing the complete Duchenne muscular dystrophy gene. *Genomics* **12**, 465-473 (1992).

11. Koenig, M. et al. The molecular basis for Duchenne versus Becker muscular dystrophy: correlation of severity with type of deletion. *Am J Hum Genet* **45**, 498-506 (1989).

12. Monaco, A.P. et al. Detection of Deletions Spanning the Duchenne Muscular-Dystrophy Locus Using a Tightly Linked DNA Segment. *Nature* **316**, 842-845 (1985).

13. Kole, R. & Krieg, A.M. Exon skipping therapy for Duchenne muscular dystrophy. *Adv Drug Deliv Rev* **87**, 104-107 (2015).

14. Birnkrant, D.J. et al. Diagnosis and management of Duchenne muscular dystrophy, part 1: diagnosis, and neuromuscular, rehabilitation, endocrine, and gastrointestinal and nutritional management. *Lancet Neurol* **17**, 251-267 (2018).

15. Mule, F., Vannucchi, M.G., Corsani, L., Serio, R. & Faussone-Pellegrini, M.S. Myogenic NOS and endogenous NO production are defective in colon from dystrophic (mdx) mice. *Am J Physiol-Gastr L* **281**, G1264-G1270 (2001).

16. Mule, F., Amato, A. & Serio, R. Gastric emptying, small intestinal transit and fecal output in dystrophic (mdx) mice. *J Physiol Sci* **60**, 75-79 (2010).

17. Feder, D. et al. Evaluation of the gastrointestinal tract in mdx mice: an experimental model of Duchenne muscular dystrophy. *Apmis* **126**, 693-699

(2018).

18. Chamberlain, J.S., Metzger, J., Reyes, M., Townsend, D. & Faulkner, J.A. Dystrophin-deficient mdx mice display a reduced life span and are susceptible to spontaneous rhabdomyosarcoma. *Faseb J* **21**, 2195-2204 (2007).

19. Wells, D.J. Tracking progress: an update on animal models for Duchenne muscular dystrophy. *Disease models & mechanisms* **11** (2018).

20. Patterson, J.K., Lei, X.G. & Miller, D.D. The pig as an experimental model for elucidating the mechanisms governing dietary influence on mineral absorption. *Exp Biol Med* **233**, 651-664 (2008).

21. Heinritz, S.N., Mosenthin, R. & Weiss, E. Use of pigs as a potential model for research into dietary modulation of the human gut microbiota. *Nutr Res Rev* **26**, 191-209 (2013).

22. Kuzmuk, K.N. & Schook, L.B. Pigs as a Model for Biomedical Sciences. *Genetics of the Pig, 2nd Edition*, 426-444 (2011).

23. Bulfield, G., Siller, W.G., Wight, P.A. & Moore, K.J. X chromosome-linked muscular dystrophy (mdx) in the mouse. *Proc Natl Acad Sci U S A* **81**, 1189-1192 (1984).

24. Larcher, T. et al. Characterization of dystrophin deficient rats: a new model for Duchenne muscular dystrophy. *PloS one* **9**, e110371 (2014).

25. Nakamura, K. et al. Generation of muscular dystrophy model rats with a CRISPR/Cas system. *Scientific reports* **4**, 5635 (2014).

26. Sui, T. et al. A novel rabbit model of Duchenne muscular dystrophy generated

by CRISPR/Cas9. *Disease models & mechanisms* **11** (2018).

27. Sharp, N.J. et al. An error in dystrophin mRNA processing in golden retriever muscular dystrophy, an animal homologue of Duchenne muscular dystrophy. *Genomics* **13**, 115-121 (1992).

28. Klymiuk, N. et al. Dystrophin-deficient pigs provide new insights into the hierarchy of physiological derangements of dystrophic muscle. *Hum Mol Genet* **22**, 4368-4382 (2013).

29. Frohlich, T. et al. Progressive muscle proteome changes in a clinically relevant pig model of Duchenne muscular dystrophy. *Scientific reports* **6** (2016).

30. Hollinger, K. et al. Dystrophin insufficiency causes selective muscle histopathology and loss of dystrophin-glycoprotein complex assembly in pig skeletal muscle. *Faseb J* **28**, 1600-1609 (2014).

31. Nonneman, D.J., Brown-Brandl, T., Jones, S.A., Wiedmann, R.T. & Rohrer, G.A. A defect in dystrophin causes a novel porcine stress syndrome. *BMC Genomics* **13**, 233 (2012).

32. Kohler, M. et al. Quality of life, physical disability, and respiratory impairment in Duchenne muscular dystrophy. *Am J Respir Crit Care Med* **172**, 1032-1036 (2005).

33. Davidson, Z.E. & Truby, H. A review of nutrition in Duchenne muscular dystrophy. *J Hum Nutr Diet* **22**, 383-393 (2009).

34. Dibner, J.J. & Richards, J.D. The digestive system: Challenges and opportunities. *J Appl Poultry Res* **13**, 86-93 (2004).

35. Pluske, J.R. et al. Maintenance of villus height and crypt depth, and enhancement of disaccharide digestion and monosaccharide absorption, in piglets fed on cows' whole milk after weaning. *Brit J Nutr* **76**, 409-422 (1996).
36. Almeida, J.A. et al. Lactose malabsorption in the elderly: Role of small intestinal bacterial overgrowth. *Scand J Gastroentero* **43**, 146-154 (2008).
37. Wang, T.C. et al. Synergistic interaction between hypergastrinemia and Helicobacter infection in a mouse model of gastric cancer. *Gastroenterology* **118**, 36-47 (2000).
38. Sipponen, P. et al. Serum levels of amidated gastrin-17 and pepsinogen I in atrophic gastritis: An observational case-control study. *Scand J Gastroentero* **37**, 785-791 (2002).
39. Cao, Q., Ran, Z.H. & Xiao, S.D. Screening of atrophic gastritis and gastric cancer by serum pepsinogen, gastrin-17 and Helicobacter pylori immunoglobulin G antibodies. *J Digest Dis* **8**, 15-22 (2007).
40. Kekki, M., Samloff, I.M., Varis, K. & Ihamaki, T. Serum Pepsinogen-I and Serum Gastrin in the Screening of Severe Atrophic Corpus Gastritis. *Scand J Gastroentero* **26**, 109-116 (1991).
41. Ricotti, V. et al. Recurrent pseudo-obstruction and sigmoid volvulus in Duchenne Muscular Dystrophy: A case report. *Neuromuscular Disord* **22**, 887-888 (2012).
42. Wang, K.K. et al. CRISPR/Cas9-mediated knockout of myostatin in Chinese indigenous Erhualian pigs. *Transgenic Res* **26**, 799-805 (2017).

43. Zou, X.D. et al. Preparation of a new type 2 diabetic miniature pig model via the CRISPR/Cas9 system. *Cell Death Dis* **10** (2019).

44. Zhou, X.Q. et al. Generation of CRISPR/Cas9-mediated gene-targeted pigs via somatic cell nuclear transfer. *Cellular and Molecular Life Sciences* **72**, 1175-1184 (2015).

FIGURES

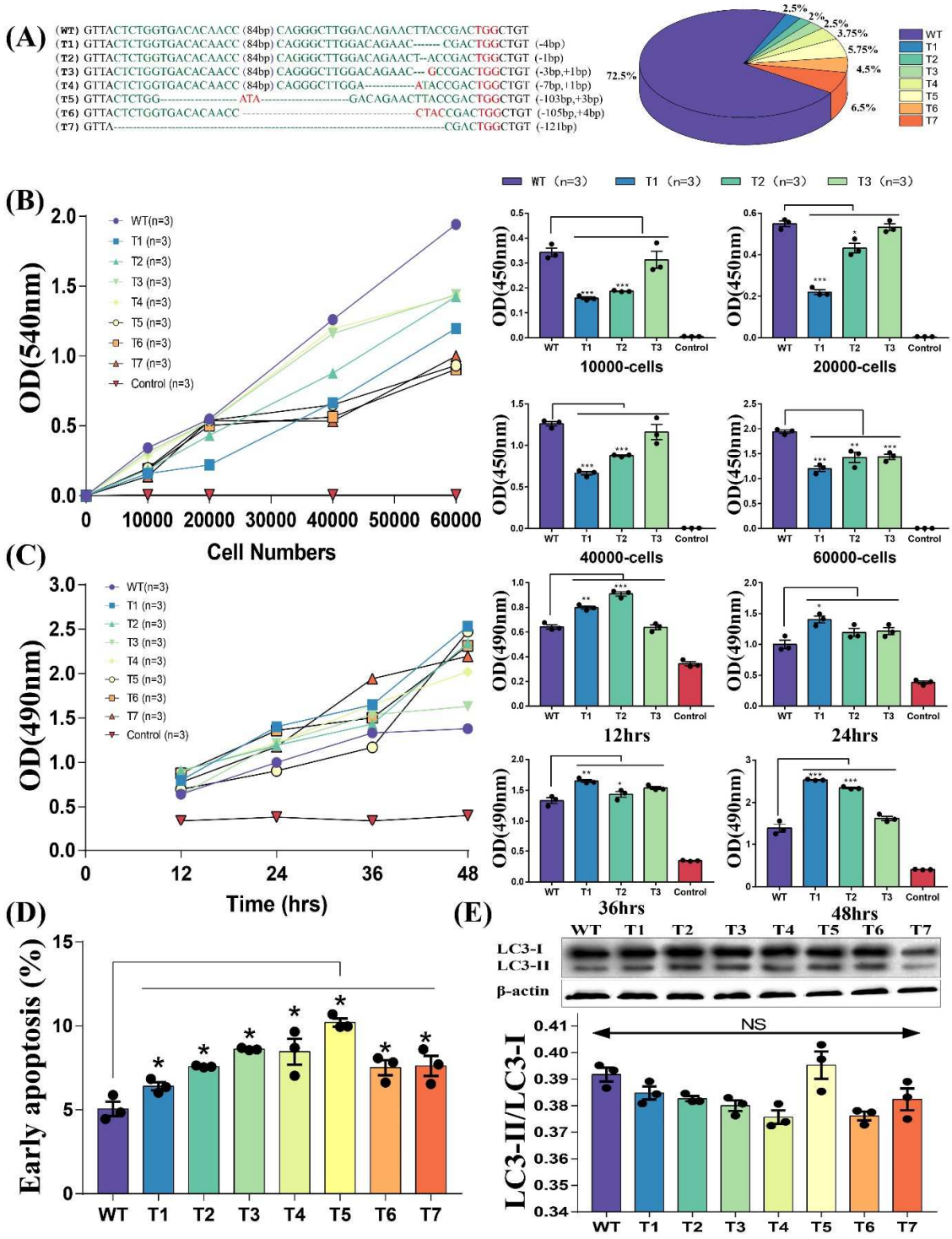

Figure 1. PFFs with *DMD* exon 51 deficiency showed impaired cell membrane integrity and early cell apoptosis. (A) Sanger sequencing of PFFs showed different mutations induced by Cas9/sgRNA electrotransfection. WT sequence is shown at the

top of the targeting sequence. PAM sequences are highlighted in red. (B) NRD uptake assay of PFF clones carrying *DMD* exon 51 mutations at different cell densities. ***P< 0.001, **P<0.01 and *P<0.05. (C) LDH activities in culture medium at different time points were measured by the LDH-kit. ***P< 0.001, **P<0.01 and *P<0.05. (D) Cell apoptosis was analyzed by flow cytometry. *P<0.05. (E) Western blotting analysis of autophagy in PFFs did not detect significant difference between WT and *DMD*-mutant PFFs.

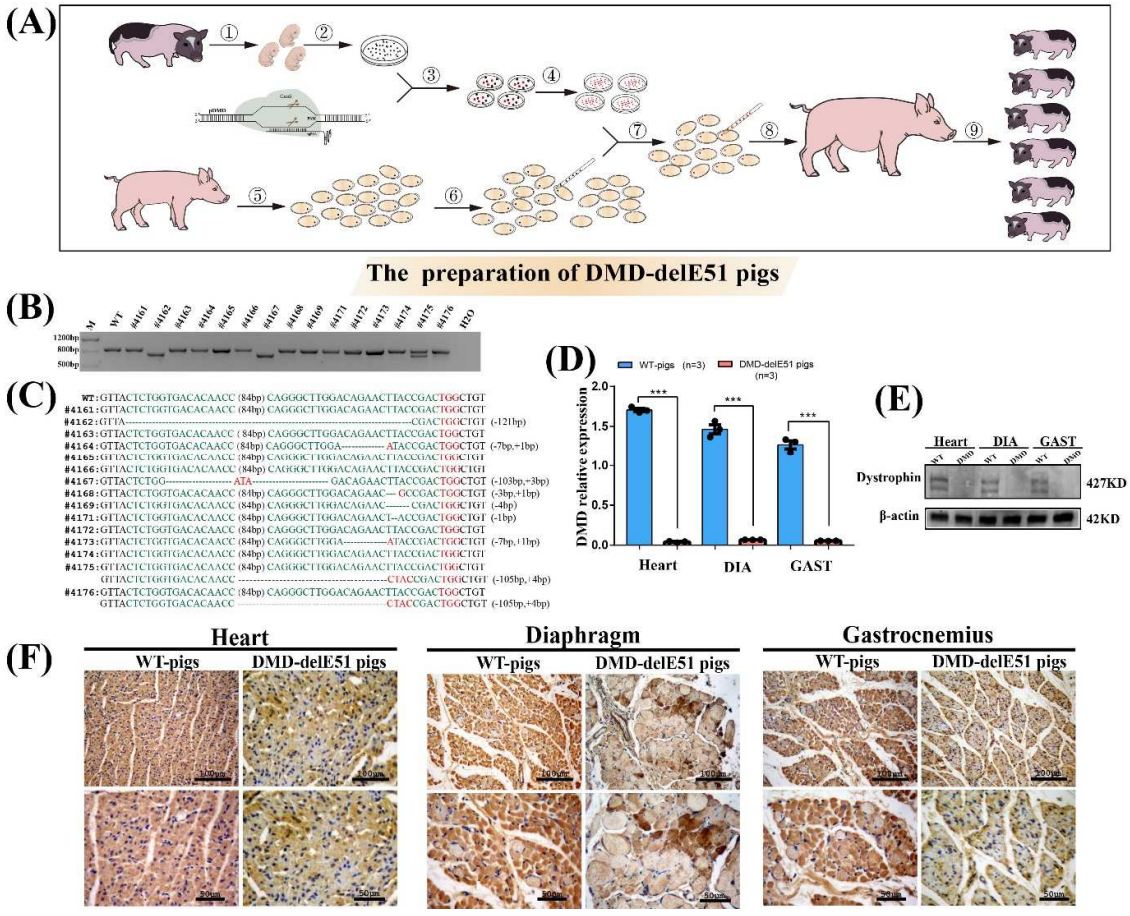

Figure 2. Generation and identification of *DMD* exon 51 defective pigs. The construction flowchart of Bama miniature pigs with edited *DMD* exon 51. ①② Isolation and culture of miniature PFFs; ③Transfection of miniature PFFs with Cas9/sgRNA; ④ Single cell clone picking and culturing; ⑤ Acquisition of oocytes; ⑥ Enucleation of oocytes; ⑦ Somatic cell nuclear transfer; ⑧ Embryo transfer; ⑨

Delivery and identification of DMD-delE51 pigs. (B) PCR analysis of *DMD* exon 51 in all piglets. (C) Mutation analysis by T-cloning and Sanger sequencing in all piglets. WT sequence is shown at the top. PAM sites are highlighted in red; target sequences are shown in green. (D) The relative expression of *DMD* mRNA in DMD-delE51 pigs and the age-matched wild-type pigs. DIA, Diaphragm; GAS, Gastrocnemius; ***P< 0.001. (E) Western blotting showed the disrupted expression of dystrophin in DMD-delE51 pigs. (F) IHC analysis of dystrophin expression in heart, diaphragm and gastrocnemius muscles. Scale bars: 50 μm and 100 μm.

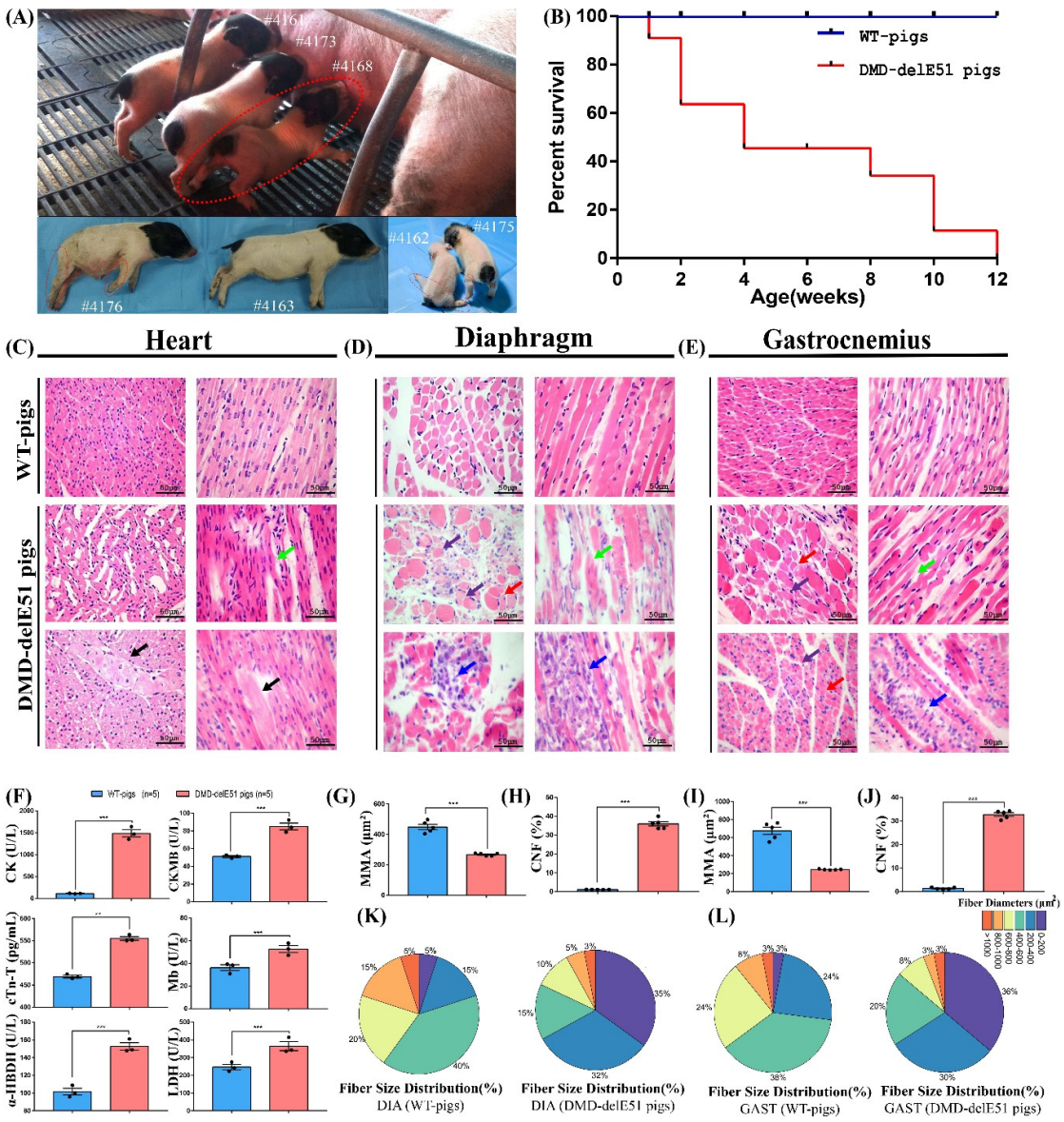

Figure 3. Development of muscular dystrophy and cardiomyopathy in DMD-delE51 pigs. (A) Piglets carrying *DMD* exon 51 mutations showed abnormal posture. (B) Survival curves of DMD-delE51 pigs and WT-pigs. (C-E) H&E staining of heart, diaphragm and gastrocnemius muscle sections from WT and DMD-delE51 pigs at the age of 12 weeks. Scale bars: 50 μm. Fiber fracture (green arrows) and hypertrophic fiber (black arrows) were seen in heart sections. Excessive fiber size variation (red arrows), central nucleated fibers (purple arrows), fiber fracture (green arrows) and inflammatory cell infiltration (blue arrows) were readily visible in muscle sections. (F) Serum biochemical profiles of WT and DMD-delE51 pigs. ***P< 0.001, **P<0.01 and

*P<0.05. (G, I) Quantification of mean fiber area (MMA) of diaphragm and gastrocnemius muscle in WT and DMD-delE51 pigs. ***P< 0.001. (H, J) Quantification of centrally nucleated fiber (CNF) percentage in WT and DMD-delE51 pigs. ***P< 0.001. (K, L) Size distribution of diaphragm and gastrocnemius muscle in WT and DMD-delE51 pigs.

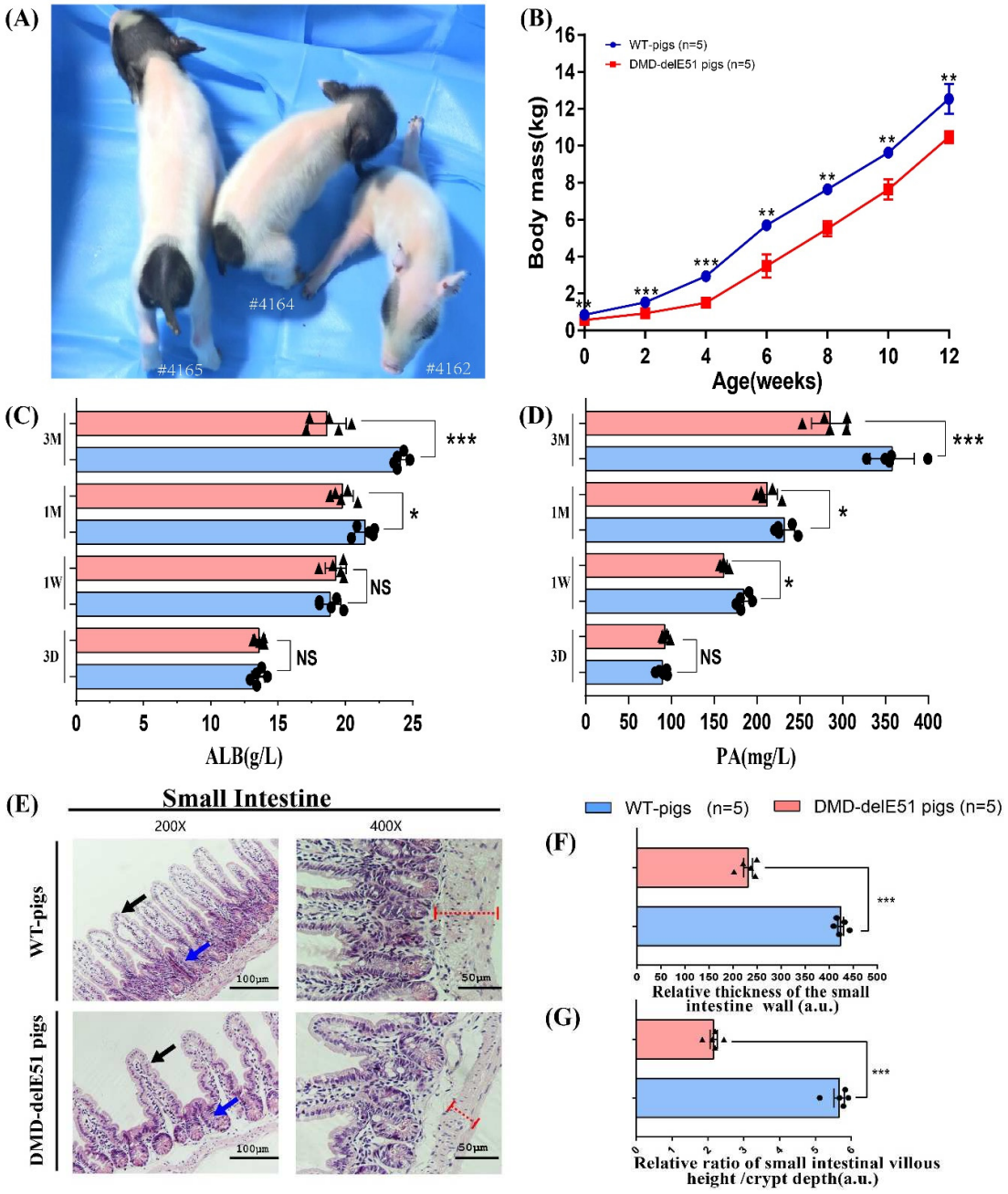

Figure 4. DMD-delE51 pigs exhibited symptoms of malnutrition. Photograph of DMD-delE51 pigs and WT control at the age of one week. (B) Body mass of DMD-delE51 and WT pigs from birth to 12 weeks of age. ***P< 0.001, **P<0.01. (C, D) Serum ALB (C) and PA (D) levels of WT and DMD-delE51 pigs. ***P< 0.001; *P<0.05. (E) H&E staining of the small intestine sections of WT and DMD-delE51 pigs. Red dotted lines indicate the thickness of the intestinal wall, black arrows indicate the height of the small intestine villi and blue arrows indicate the depth of the small

intestine crypt. Scale bars: 50 μm and 100 μm. (F) The relative thickness of small intestinal wall in WT and DMD-delE51 pigs. *** $p < 0.01$. (G) The relative ratio of small intestine villus height/crypt depth of WT and DMD-delE51 pigs. *** $p < 0.01$.

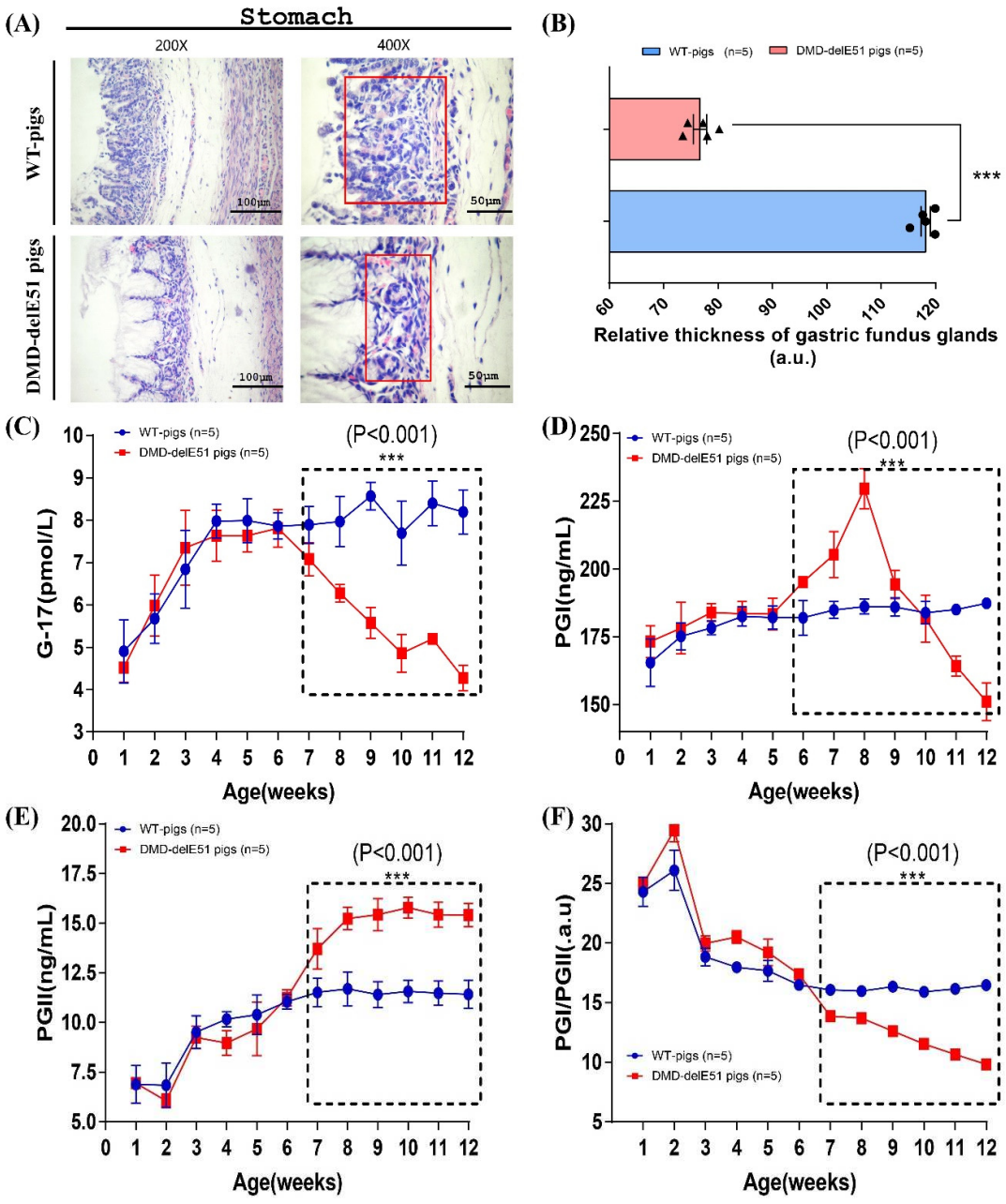

640

641 **Figure 5. DMD-delE51 pigs suffered from atrophic gastritis.** (A) H&E staining of
642 stomach sections from WT and DMD-delE51 pigs at the age of 12 weeks. The
643 thickness of gastric fundus glands (red rectangle) was reduced in DMD-delE51 pigs.
644 Scale bars: 50 μm and 100 μm. (B) Quantification of the relative thickness of gastric
645 fundus glands in WT and DMD-delE51 pigs. *** $p < 0.01$. (C) Measurements of serum
646 G-17 in WT and DMD-delE51 pigs. ***$P< 0.001$. (D) Measurement of serum PGI in
647 WT and DMD-delE51 pigs. ***$P< 0.001$. (E) Measurement of serum PGII in WT and

DMD-delE51 pigs. ***P< 0.001. (F) The ratio of PGI/PGII in WT and DMD-delE51 pigs.

*** $p < 0.01$.

Supplementary Information

Supplementary Table 1: List of putative off-target sites (PAM sequences are labeled in blue. Base substitutions are shown in red.)

sgRNA	CTTGGACAGAACTTACCGACTGG
OTS1	CCAGTACAGAACTTACAGACCGG
OTS2	CTTTGATAGGACTTACCGATTAG
OTS3	CTTCTCCAGAACTTACCGCCCAG
OTS4	CTTGTACAGAAATCACCGACCAG
OTS5	CTTGGACACATCTTACCAACAGG
OTS6	CCTGTACAGAACTTACCTATGAG
OTS7	CTTGGCCAGCATTTACCGTCAGG
OTS8	ATTTGACAGAACATACCAACAGG

Supplementary Table 2: List of primers for PCR amplification of off-target sites.

Primers	Sequences (5' to 3')	Amplicon (bp)
DMD- sgRNA-OTS1	AAGGAAATTGAGACTCAGAGAAGA	502
	TGCTTTTCATTGGCTCTGGC	
DMD- sgRNA-OTS2	TGCCAGTGTGGTTGGTTTCT	551
	CCAGTCCATTCCCCCATCAC	
DMD - sgRNA-OTS3	GTTTACCGCAGACCCACAGA	589
	GTGCGTAGAGACCCAAACCA	
DMD - sgRNA-OTS4	GGCTGGTCATGGTTAGCACT	522
	CTGAACACCCTTCCTCCACC	
DMD - sgRNA-OTS5	TTTGACCCCAATCCATGCGT	577
	TGCTCTATGCCACTTCGCTT	
DMD - sgRNA-OTS6	TGTGTCTTGGTGGGTGATGG	508
	GTGTGGATGGGTGTATGCCA	
DMD - sgRNA-OTS7	AGGGGCTTATGCTTGTGGTC	522
	TCAGAAGCCTGCCCTTCATG	
DMD - sgRNA-OTS8	GGTCCTGACCCTTTGGATGT	593
	AGGCTGAATTATCTGAGTGCCA	

Supplementary Table 3: Identification and classification of PFFs carrying different mutations in *DMD* exon 51.

Types of clone cell	Numbers	Percentage (%)
Wild type (WT)	290	72.50
DMD-KO-Type 1 (T1)	10	2.50
DMD-KO-Type 2 (T2)	8	2.00
DMD-KO-Type 3 (T3)	10	2.50
DMD-KO-Type 4 (T4)	15	3.75
DMD-KO-Type 5 (T5)	23	5.75
DMD-KO-Type 6 (T6)	18	4.50
DMD-KO-Type 7 (T7)	26	6.50
In total	400	100.00

Supplementary Table 4: Analysis of blastocyst development rate of DMD exon 51-modified PFFs.

Cell Clone Types	SCNT Repeats	Nuclear Cell Clones Number	Blastocyst Number	Blastocyst Development Rate（%）
T1	1	80	12	15.00
	2	80	14	17.50
	3	80	13	16.30
T2	1	80	14	17.50
	2	80	14	17.50
	3	80	13	16.30
T3	1	80	12	15.00
	2	80	18	22.50
	3	80	13	16.30
T4	1	80	13	16.30
	2	80	12	15.00
	3	80	18	22.50
T5	1	80	15	18.80
	2	80	13	16.30
	3	80	12	15.00
T6	1	80	15	18.80
	2	80	14	17.50
	3	80	15	18.80
T7	1	80	14	17.50
	2	80	15	18.80
	3	80	15	18.80
WT	1	80	17	21.30
	2	80	17	21.30
	3	80	14	17.50

Supplementary Table 5: SCNT results for the generation of DMD-delE51 pigs.

Target gene	Transferred embryos	No. recipients	No.(%) pregnancies	No. born	No. (%) mutants
DMD	200	1	1	4	2
	200	1	0	0	0
	200	1	1	4	3
	200	1	0	0	0
	200	1	1	7	4
Total	1000	5	3	15	9

Supplementary Table 6: List of primers used for RT-PCR.

RT-*DMD*-F (5'-3')	CCCTGGACTGACCACTAT
RT-*DMD*-R (5'-3')	CTCTGTGATTTTATAACTCG
RT-*GAPDH*-F (5'-3')	ATCCTGGGCTACACTGAGGA
RT-*GAPDH*-R (5'-3')	TGTCGTACCAGGAAATGAGCT

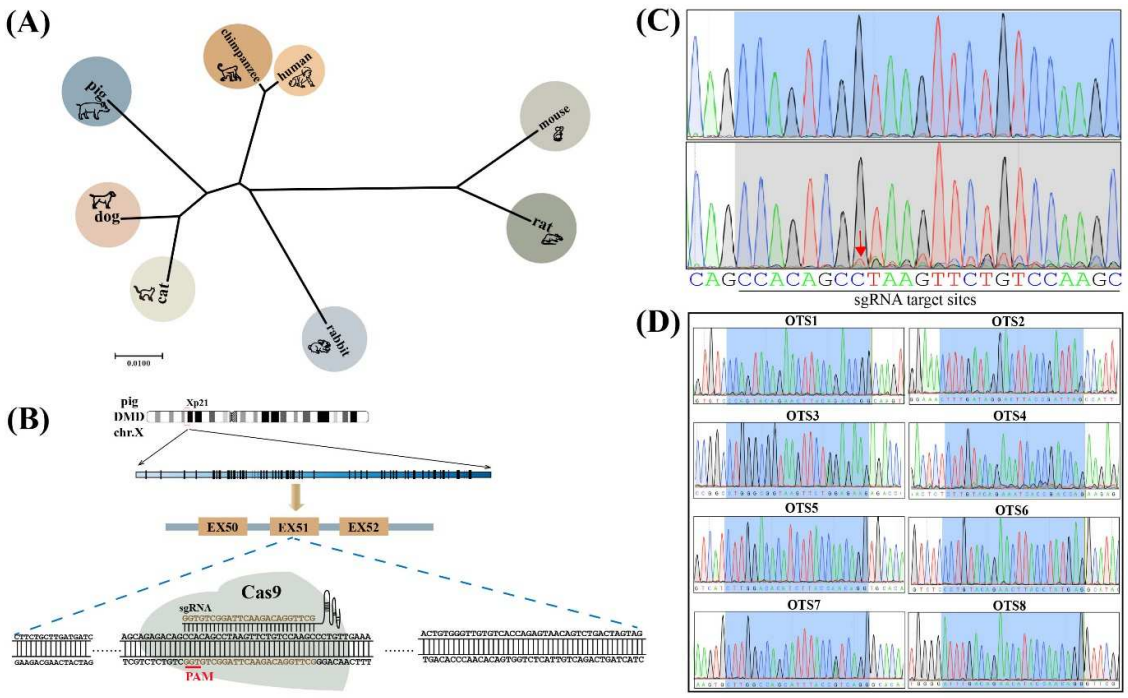

Supplementary Figure 1. **Sequence analysis of pig dystrophin and design of CRISPR-targeting strategy**. (A) Comparison of amino acid sequences of dystrophin proteins among different species. (B)Schematic representation of the sgRNA targeting porcine *DMD* exon 51. PAM is highlighted in red. (C) Sanger sequencing traces of PCR amplicons from WT and electrotransfected PFFs. The cleavage sites are labeled with a red arrow. (D) The analysis of off-target sites (OTS). The corresponding sequencing chromatograms for the top OTS are shown.

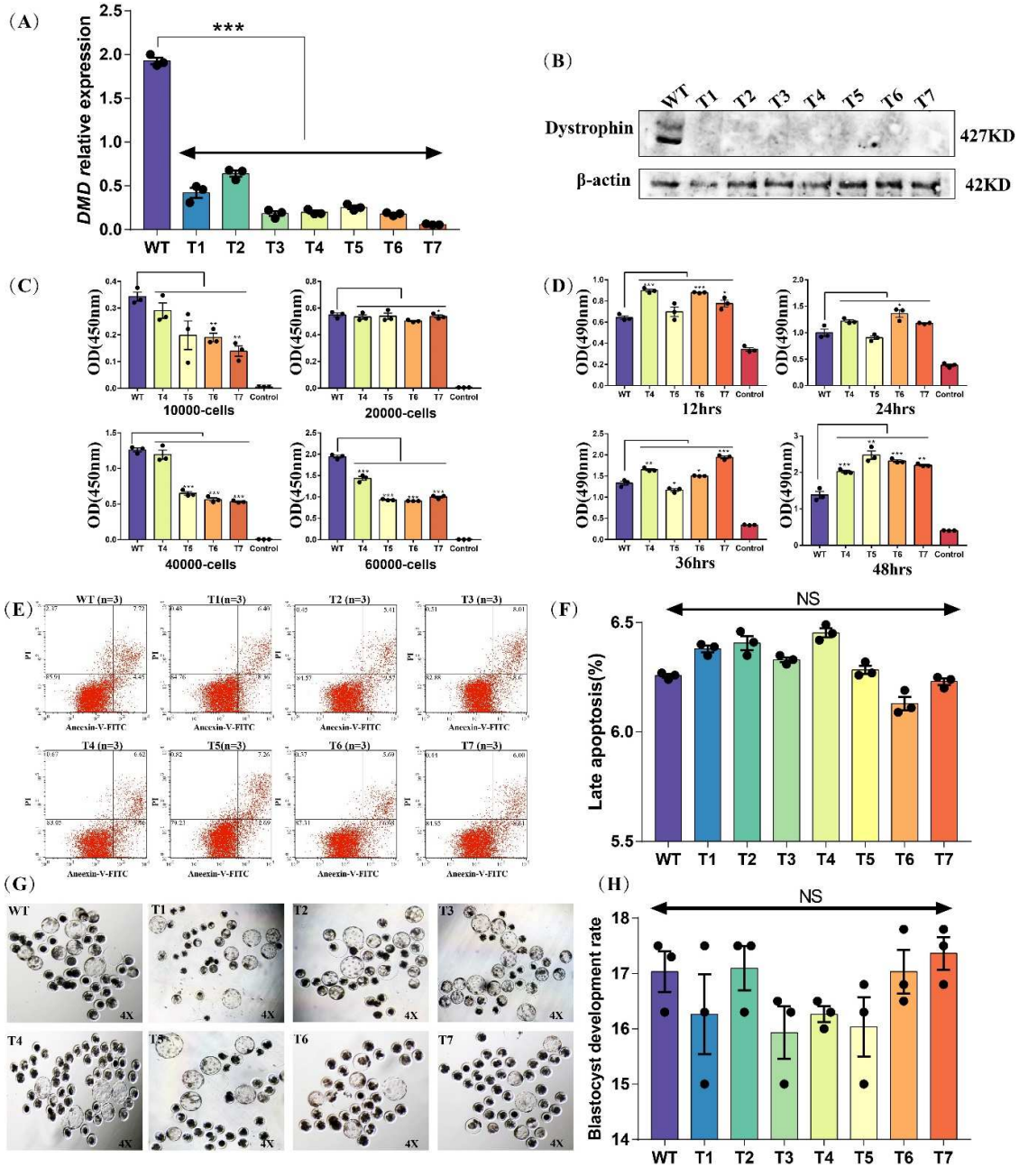

Supplementary Figure 2. Analysis of PFFs with *DMD* mutations. The relative expression of *DMD* mRNA in DMD-edited and WT PFFs. ***P< 0.001. (B) Western blotting analysis of dystrophin expression in DMD-modified and WT PFFs. (C) NRD uptake analysis of PFF cell clones carrying DMD exon 51 mutations at different cell densities; ***P< 0.001, **P<0.01 and *P<0.05. (D) LDH activity in culture medium at

different time periods. ***P< 0.001, **P<0.01 and *P<0.05. (E, F) Cell apoptosis analyzed by flow cytometry. (G) Representative images of blastocysts at 8.5 days after nuclear transfer. PFFs with DMD exon 51 modified could develop normally into blastocysts. (H) The analysis of blastocyst development rate of PFFs carrying DMD exon 51mutations. NS, no significant.

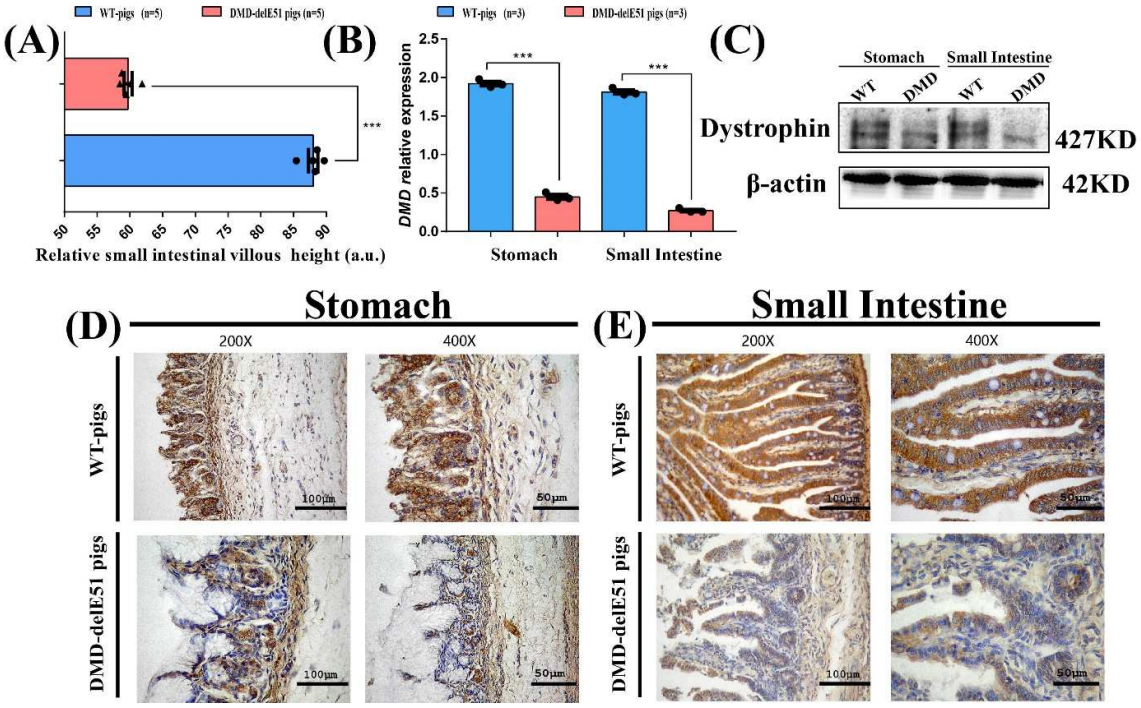

Supplementary Figure 3. Dystrophin expression in porcine stomach and small intestine. (A) The relative height of small intestine villus in WT and DMD-delE51 pigs. *** p < 0.01. (B) The relative expression of *DMD* mRNA in stomach and small intestine from DMD-delE51 pigs and the age-matched wild-type pigs; ***P< 0.001. (C) Western blotting analysis of dystrophin in stomach and small intestine of WT and DMD-delE51 pigs. (D, E) IHC staining of dystrophin in stomach (D) and small intestine (E) of pigs. Scale bars: 50 μm and 100 μm.

Figures

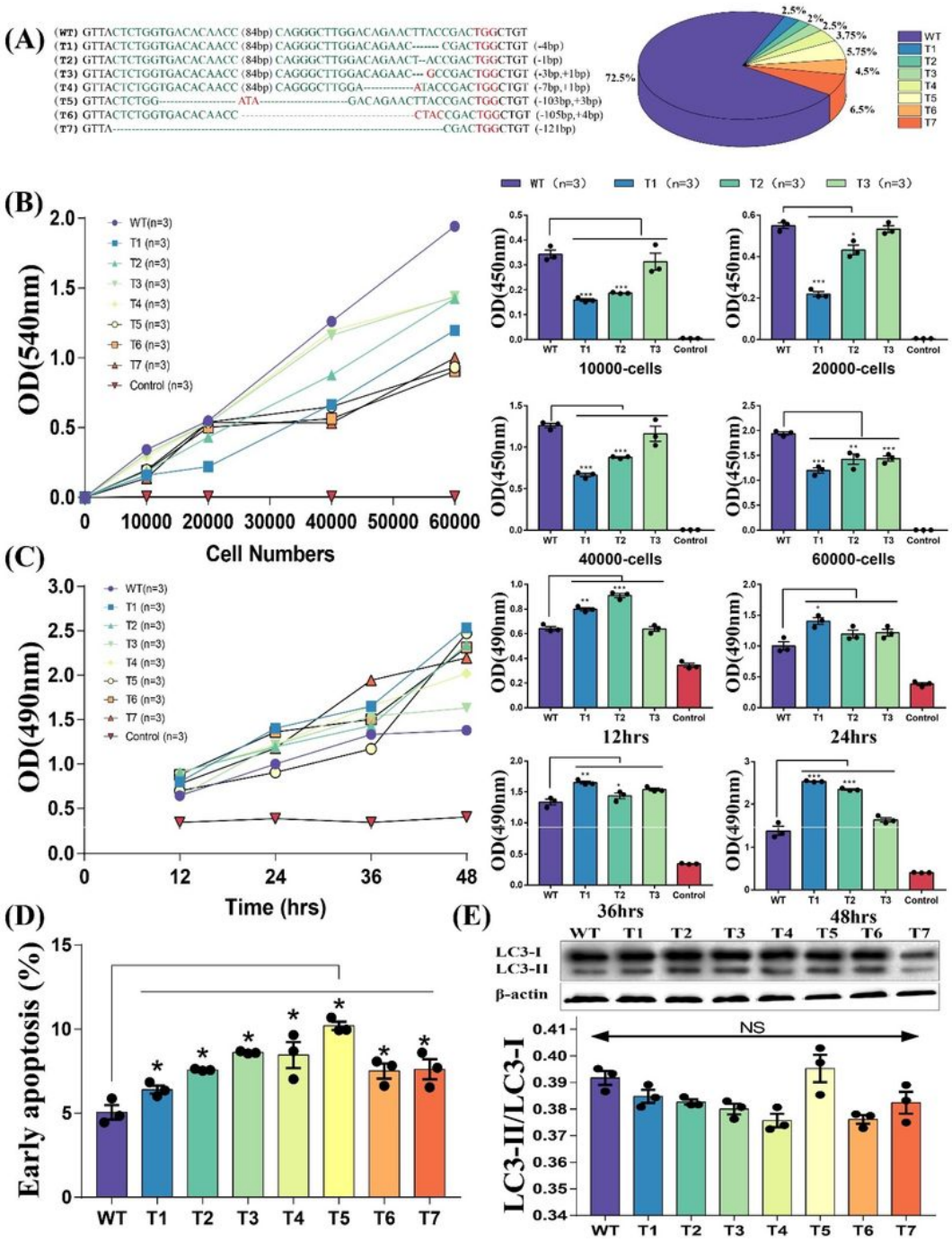

Figure 1

PFFs with DMD exon 51 deficiency showed impaired cell membrane integrity and early cell apoptosis. (A) Sanger sequencing of PFFs showed different mutations induced by Cas9/sgRNA electrotransfection. WT sequence is shown at the top of the targeting sequence. PAM sequences are highlighted 582 in red. (B)

NRD uptake assay of PFF clones carrying DMD exon 51 mutations at different cell densities. ***P< 0.001, **P<0.01 and *P<0.05. (C) LDH activities in culture medium at different time points were measured by the LDH-kit. ***P< 0.001, **P<0.01 and *P<0.05. (D) Cell apoptosis was analyzed by flow cytometry. *P<0.05. (E) Western blotting analysis of autophagy in PFFs did not detect significant difference between WT and DMD-mutant PFFs.

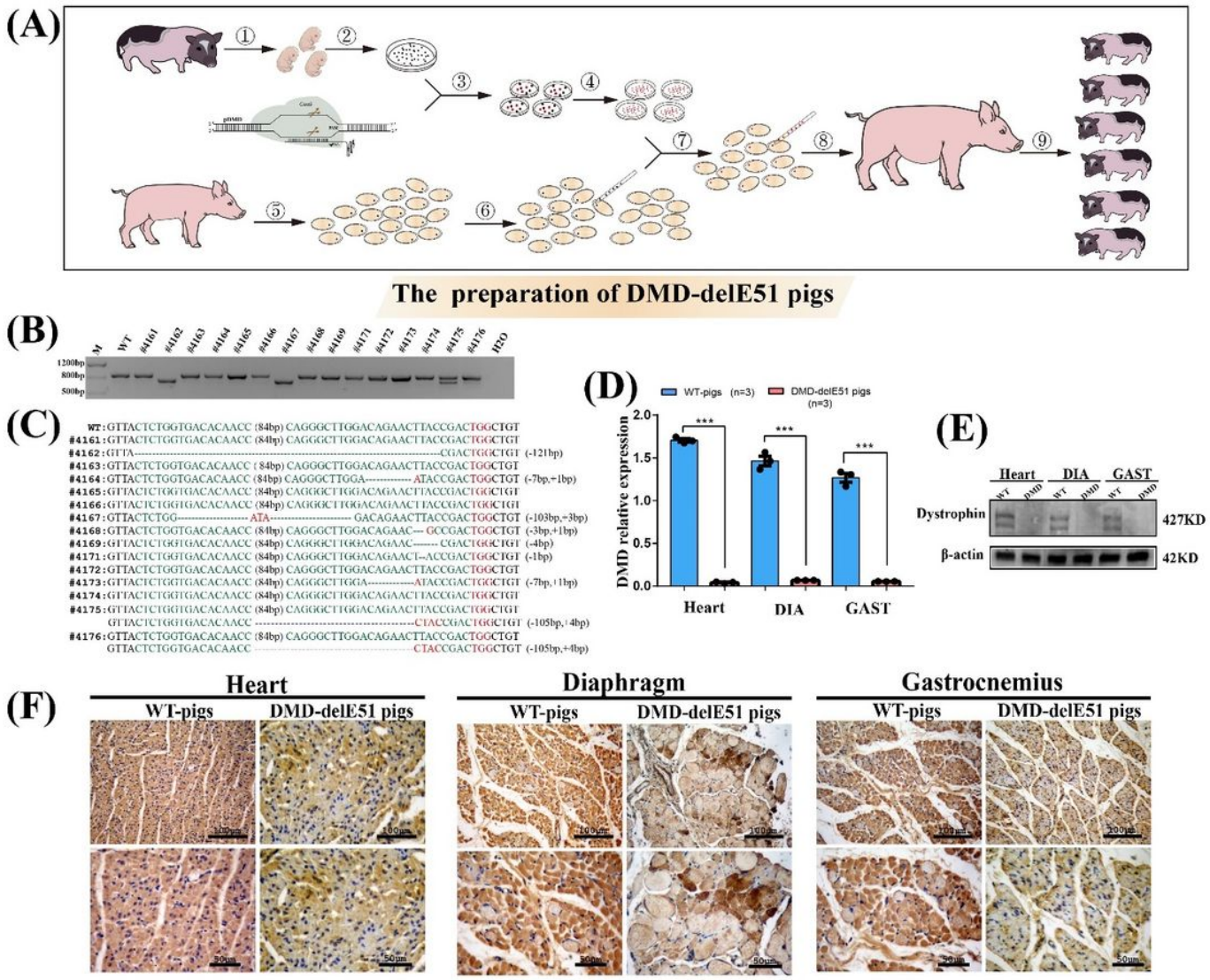

Figure 2

Generation and identification of DMD exon 51 defective pigs. The construction flowchart of Bama miniature pigs with edited DMD exon 51. ①② Isolation and culture of miniature PFFs; ③Transfection of miniature PFFs with Cas9/sgRNA; ④ Single cell clone picking and culturing; ⑤ Acquisition of oocytes; ⑥ Enucleation of oocytes; ⑦ Somatic cell nuclear transfer; ⑧ Embryo transfer; ⑨ Delivery and identification of DMD-delE51 pigs. (B) 597 PCR analysis of DMD exon 51 in all piglets. (C) Mutation analysis by T-cloning and Sanger sequencing in all piglets. WT sequence is shown at the top. PAM sites are highlighted in red;

target sequences are shown in green. (D) The relative expression of DMD mRNA in DMD-delE51 pigs and the age-matched wild-type pigs. DIA, Diaphragm; GAS, Gastrocnemius; ***P< 0.001. (E) Western blotting showed the disrupted expression of dystrophin in DMD-delE51 pigs. (F) IHC analysis of dystrophin expression in heart, diaphragm and gastrocnemius muscles. Scale bars: 50 μm and 100 μm.

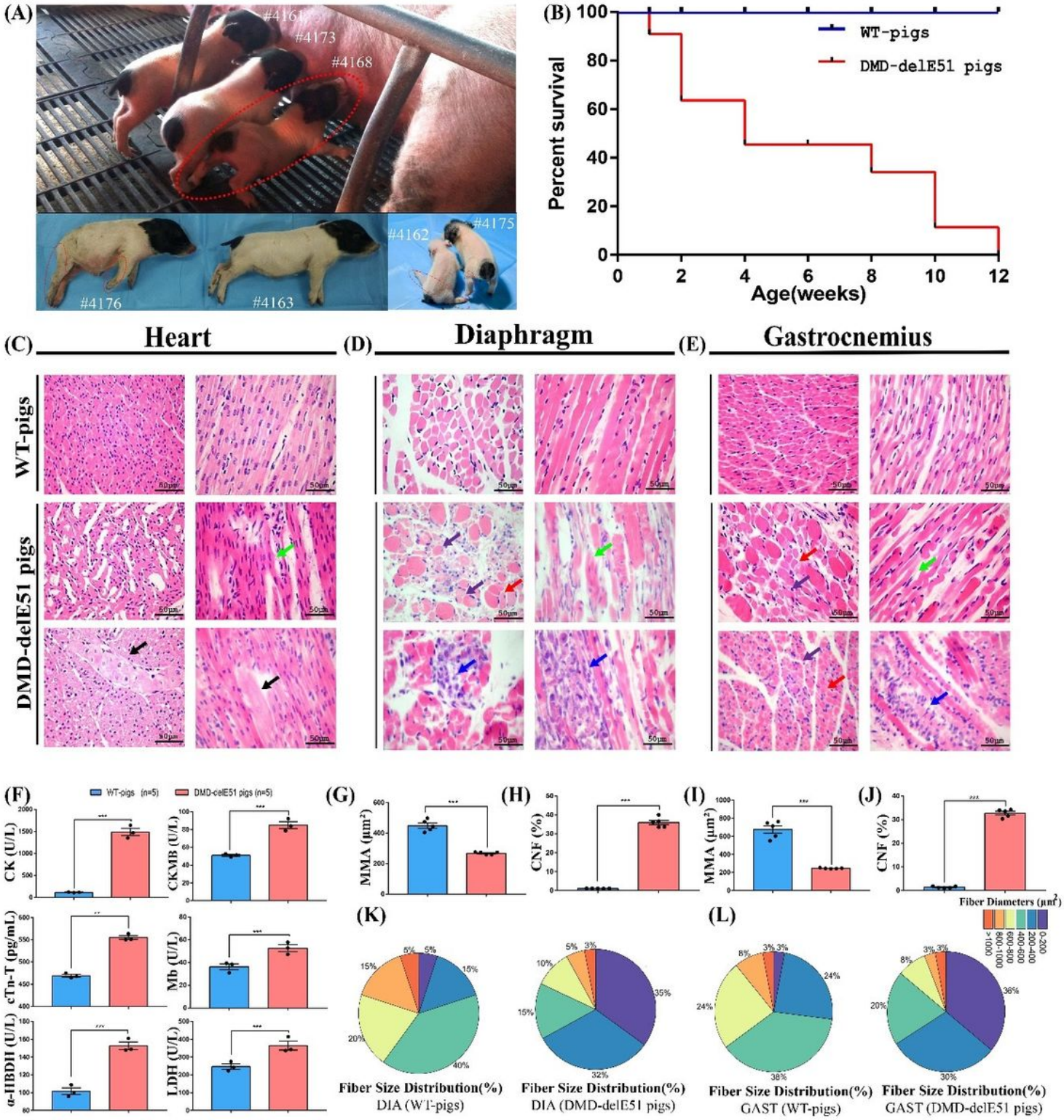

Figure 3

Development of muscular dystrophy and cardiomyopathy in DMD-delE51 pigs. (A) Piglets carrying DMD exon 51 mutations showed abnormal posture. (B) Survival curves of DMD-delE51 pigs and WT-pigs. (C-E) H&E staining of heart, diaphragm and gastrocnemius muscle sections from WT and DMD-delE51 pigs at the age of 12 weeks. Scale bars: 50 μm. Fiber fracture (green arrows) and hypertrophic fiber (black arrows) were seen in heart sections. Excessive fiber size variation (red arrows), central nucleated fibers (purple arrows), fiber fracture (green arrows) and inflammatory cell infiltration (blue arrows) were readily visible in muscle sections. (F) Serum biochemical profiles of WT and DMD-delE51 pigs. ***P< 0.001, **P<0.01 and *P<0.05. (G, I) Quantification of 617 mean fiber area (MMA) of diaphragm and gastrocnemius muscle in WT and DMD-delE51 pigs. ***P< 0.001. (H, J) Quantification of centrally nucleated fiber (CNF) percentage in WT and DMD-delE51 pigs. ***P< 0.001. (K, L) Size distribution of diaphragm and gastrocnemius muscle in WT and DMD-delE51 pigs.

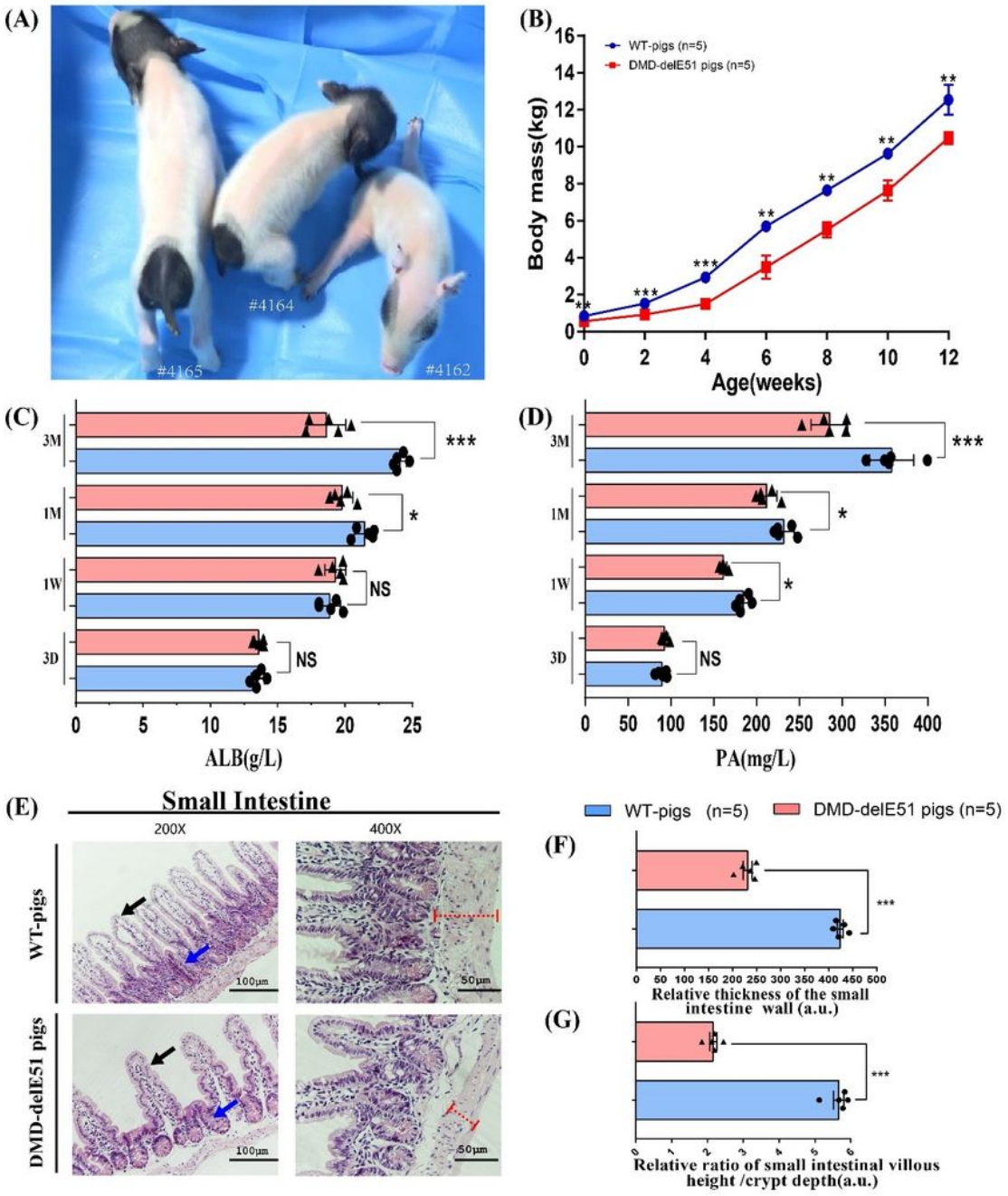

Figure 4

DMD-delE51 pigs exhibited symptoms of malnutrition. Photograph of DMD-delE51 pigs and WT control at the age of one week. (B) Body mass of DMD-delE51 and WT pigs from birth to 12 weeks of age. ***P< 0.001, **P<0.01. (C, D) Serum ALB (C) and PA (D) levels of WT and DMD-delE51 pigs. ***P< 0.001; *P<0.05. (E) H&E staining of the small intestine sections of WT and DMD-delE51 pigs. Red dotted lines indicate the thickness of the intestinal wall, black arrows indicate the height of the small intestine villi and

blue arrows indicate the depth of the small intestine crypt. Scale bars: 50 μm and 100 μm. (F) The relative 633 thickness of small intestinal wall in WT and DMD-delE51 pigs. *** $p < 0.01$. (G) The relative ratio of small intestine villus height/crypt depth of WT and DMD-delE51 pigs. *** $p < 0.01$.

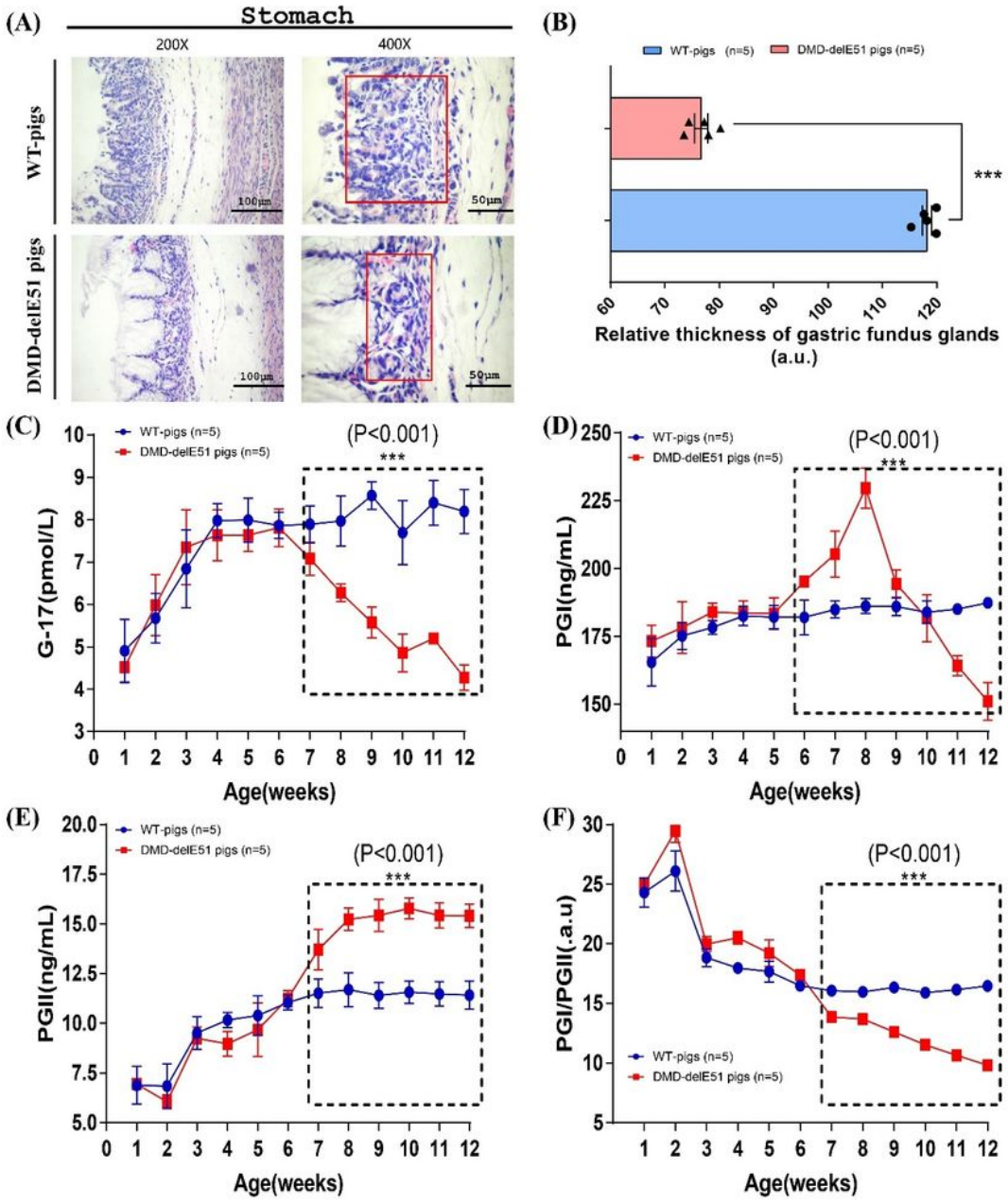

Figure 5

MD-delE51 pigs suffered from atrophic gastritis. (A) H&E staining of stomach sections from WT and DMD-delE51 pigs at the age of 12 weeks. The thickness of gastric fundus glands (red rectangle) was

reduced in DMD-delE51 pigs. Scale bars: 50 μm and 100 μm. (B) Quantification of the relative thickness of gastric fundus glands in WT and DMD-delE51 pigs. *** $p < 0.01$. (C) Measurements of serum G-17 in WT and DMD-delE51 pigs. ***$P< 0.001$. (D) Measurement of serum PGI in WT and DMD-delE51 pigs. ***$P< 0.001$. (E) Measurement of serum PGII in WT and DMD-delE51 pigs. ***$P< 0.001$. (F) The ratio of 648 PGI/PGII in WT and DMD-delE51 pigs. *** $p < 0.01$.